# Reorientation and breakup effects in polarized $^{7}$Li+$^{12}$C elastic scattering

E. E. Bartosz, N. Keeley, P. D. Cathers, M. W. Cooper, K. W. Kemper, and F. Maréchal*
*Department of Physics, The Florida State University, Tallahassee, Florida 32306*

K. Rusek
*Department of Nuclear Reactions, The Andrzej Sołtan Institute for Nuclear Studies, Hoża 69, PL-00-681 Warsaw, Poland*
(Received 13 March 2001; published 8 June 2001)

A complete set of analyzing powers has been obtained for $^{12}$C($^{7}\vec{\text{Li}}$,$^{7}$Li)$^{12}$C elastic scattering at a bombarding energy of 34 MeV. Optical model calculations using standard forms for the spin-orbit and tensor potentials are unable to simultaneously describe all the available data. However, coupled-discretized-continuum-channels (CDCC) calculations using cluster-folding model form factors provide a reasonable overall description of the data with only two adjustable parameters. Reorientation effects are extremely important in obtaining a good description of the analyzing powers, with the reorientation coupling of the $^{7}$Li ground state being a major contributor to all the analyzing powers and the main source of the second-rank tensor analyzing powers $T_{20}$, $T_{21}$, and $T_{22}$. The failure of optical model calculations to describe the second rank data implies that the effect of this reorientation coupling cannot be described accurately by means of a dynamic polarization potential constrained to be of the standard forms. The CDCC calculations also demonstrate the effect of coupling to the $\alpha$-$t$ continuum on the analyzing powers.

DOI: 10.1103/PhysRevC.64.014606 PACS number(s): 24.70.+s, 25.70.Bc, 24.10.Ht, 24.10.Eq

## I. INTRODUCTION

Recently, a complete set of analyzing powers has been obtained for the elastic scattering of polarized $^{7}$Li by a $^{12}$C target at a bombarding energy of 34 MeV. Angular distributions for $^{T}T_{10}$ and $^{T}T_{30}$ have been published previously [1], but we present the full data set here for the first time. Previous measurements of third-rank analyzing powers, for 44 MeV $^{7}$Li+$^{120}$Sn [2] and 44 MeV $^{7}$Li+$^{26}$Mg [3], were limited to a single analyzing power, $^{T}T_{30}$, which is a linear combination of two other third-rank analyzing powers, $iT_{31}$ and $iT_{33}$:

$$^{T}T_{30} = -\left(\sqrt{\tfrac{3}{4}}iT_{31} + \sqrt{\tfrac{5}{4}}iT_{33}\right). \quad (1)$$

The first complete set of $^{7}$Li analyzing powers has recently been reported, for $^{7}$Li + $^{4}$He elastic scattering [4]. The current data constitute the first complete set of $^{7}$Li analyzing powers for a target where elastic transfer does not play a role.

Such a comprehensive data set as that presented here provides an excellent opportunity to investigate the relative importance of reorientation (due to the large ground-state quadrupole moment of $^{7}$Li) and breakup (due to the weak $\alpha$-$t$ binding energy of $^{7}$Li) couplings for the elastic scattering. The ground-state reorientation coupling in $^{7}$Li has previously been shown to have a significant effect on the elastic scattering cross section [5] and to be the main source of the second-rank tensor analyzing powers in polarized $^{7}$Li elastic scattering from a $^{120}$Sn target [2] and a $^{26}$Mg target [3], both at bombarding energies of 44 MeV. It is of interest to establish whether the second-rank analyzing powers are still mainly produced by the ground-state reorientation coupling at the higher relative bombarding energy with respect to the Coulomb barrier of the current data.

The current data also afford the opportunity for comparison with the polarized $^{6}$Li+$^{12}$C data of Reber *et al.* [6] for a $^{6}$Li bombarding energy of 30 MeV. The elastic scattering cross section and first- and second-rank analyzing powers of the current data set are compared with those of Reber *et al.* in Fig. 1. Similar behavior to that observed for the elastic scattering of $^{6,7}$Li+$^{12}$C at about 20 MeV [7,8] and $^{6,7}$Li +$^{26}$Mg at 44 MeV [3,9] is found, namely that, while the first-rank analyzing powers show oscillatory structure of comparable magnitude for both isotopes, the second-rank analyzing powers for $^{7}$Li are considerably larger and more structured than those of $^{6}$Li.

In this paper we present the results of an extensive optical model search that attempted to fit the cross section and analyzing power data simultaneously using standard forms for the central, spin-orbit, and second- and third-rank tensor potentials. We were unable to obtain a good description of all the elastic scattering observables using this procedure, the main problem being an inability to describe the second-rank tensor analyzing powers without destroying previous good agreement with the vector and third-rank analyzing powers.

To address the shortcomings of the optical model calculations, coupled-discretized-continuum-channels (CDCC) calculations using cluster-folding (CF) model form factors were carried out. These calculations included couplings to the first excited state, $7/2^{-}$ and $5/2^{-}$ resonances of $^{7}$Li and the $L=0,1,3$ $\alpha$-$t$ continuum. They provide a reasonably good overall description of the data and suggest that the second-rank analyzing powers are in large part due to coupling to the ground-state reorientation of $^{7}$Li rather than the $\alpha$-$t$ breakup. This result, together with the failure of the op-

*Present address: Institut de Recherches Subatomiques, BP28, F-67037 Strasbourg, Cedex 02, France.

 

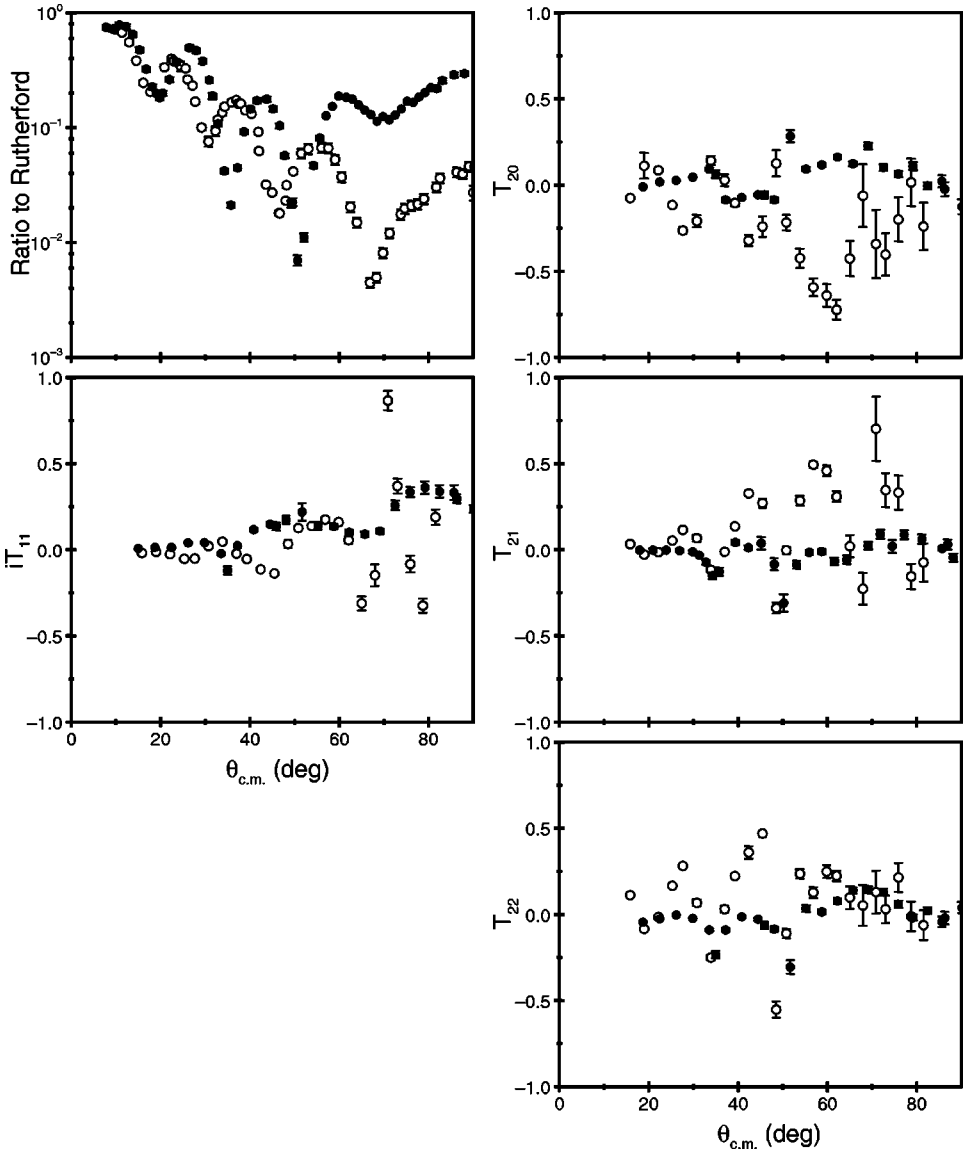


FIG. 1. Comparison of previously measured cross section and analyzing power data for 30 MeV $^{6}$Li+$^{12}$C (filled circles) with the current $^{7}$Li+$^{12}$C data (open circles).

tical model to provide an adequate description of all the polarization observables, suggests that the reorientation coupling cannot be adequately represented with a dynamic polarization potential (DPP) of conventional form, as is generally assumed for loosely bound projectiles.

A description of the experimental method used to obtain these data is contained in Sec. II. In Sec. III the optical model calculations are described and the results of the best fit to all the data are presented. In Sec. IV the CDCC calculations are briefly described and the results are compared with the elastic scattering data. In Sec. V we discuss the results of the optical model and CDCC calculations and present our conclusions.

## II. EXPERIMENTAL METHOD

Details of the procedure used to obtain a polarized $^{7}$Li beam have been published elsewhere [10,4], so only a brief outline will be given here. The Florida State University (FSU) optically pumped polarized lithium ion source (OPPLIS) [11] was used to produce a $^{7}$Li beam preferentially in one of the $^{7}$Li magnetic substates $m_I=\frac{3}{2}$, $\frac{1}{2}$, $-\frac{1}{2}$, and $-\frac{3}{2}$, referred to as state $N_m$. The data acquisition system cycled the polarization state of the beam automatically through the unpolarized state and each of the polarized states $N_m$ as required, spending approximately 3 min in each state. After ionization and charge exchange in a cesium charge exchange cell, the beam passed through the magnetic field of a Wien filter to properly orient the spin quantization axis. It was then accelerated by the FSU Super FN Tandem accelerator to an energy of 34 MeV. The scattering chambers consisted of an evacuated 85 cm chamber followed by a helium-filled chamber at 380 Torr. The reaction chamber contained a self-supporting $^{12}$C target of areal density 400 $\mu$g/cm$^2$. Reaction products were detected with four silicon surface barrier $\Delta E$-$E$ telescopes placed symmetrically to the left and right of the beam and rotated about the target. All four $E$ detectors were 1000 $\mu$m thick, while the inner and outer $\Delta E$ detectors were 75 $\mu$m and 40 $\mu$m thick, respectively. The 34 MeV beam was slowed to 31.5 MeV in the helium target volume

by passing through a Havar foil, which isolated the helium gas from the evacuated 85 cm chamber, and 26 cm of gas to the center of the helium-filled chamber. The typical $^7Li^{3+}$ beam current on target was 60 nA.

The analyzing power data reported here were taken in the 85 cm scattering chamber, while the beam polarization on target was measured and monitored in the helium-filled chamber using the secondary standards established by Cathers *et al.* [10] for the reaction $^4He(\vec{^7Li},^7Li)$. The specific beam polarization states, spin quantization axis orientations, and resulting equations used to measure the analyzing powers and measure the polarization on target have been specified elsewhere [4] and will be omitted here. Typical beam polarizations were $t_{10}=0.50\pm0.02$, $t_{20}=0.55\pm0.02$, and $t_{30}=0.47\pm0.03$. The lithium beam polarizations produced by OPPLIS have been found over several years of operation to be stable to within $\pm5\%$ when the optimum laser power level for the optical pumping is maintained. This stability was observed during the present work.

## III. OPTICAL MODEL CALCULATIONS

The optical model calculations were carried out using the code HERMES [12], which allows the inclusion of spin-orbit and second- and third-rank tensor potentials in addition to the central potential. The spin-orbit potential employed was of the usual Thomas form, while the second-rank tensor potential was of the second derivative form suggested by Raynal [13]. The third-rank tensor potential was also of second derivative form, of the Irshad and Robson type [14]. The use of a second derivative form for the third-rank potential, rather than the third derivative form suggested by a natural progression from the first derivative spin orbit to the second derivative second-rank tensor potentials, was guided by the work of Mukhopadhyay *et al.* [15] who derived a third-rank potential of this form based on $\alpha$-$t$ cluster folding arguments. Standard Woods-Saxon forms were used for the central potential. Both real and imaginary parts were available for each potential, providing in principal a total of 24 parameters to be determined by the data.

Merely attempting to minimize $\chi^2$ in order to extract the interaction potential was found to be inadequate, due to the large size of the parameter space involved and the number of observables that must be described simultaneously. A semi-automated procedure was adopted, whereby large numbers of optical model calculations were carried out varying the parameters in a systematic way, and the results are plotted against the data. The quality of the resultant fit was then assessed subjectively.

The central potential (set IX) of Vineyard *et al.* [16] was used as a basis in all the searches, as it provides a good description of the elastic scattering cross section. Extensive searches using various combinations of the spin-orbit and second- and third-rank tensor potentials failed to find a simultaneous description of all the data. A good description of the vector analyzing power $iT_{11}$ could be obtained using a central plus spin-orbit potential alone, but the inclusion of a second-rank tensor potential in an attempt to also describe the second-rank tensor analyzing powers destroyed this good agreement. The parameters of the spin-orbit potential are given as set I of Table I, and the results are compared with the data in Fig. 2, where they are denoted by the dashed curve.

TABLE I. Optical model parameters obtained from the HERMES calculations. The radius parameters are given as $r_x$ according to the convention, $R_x=r_xA_T^{1/3}$. The Coulomb radius parameter, $r_c$, was 2.09 fm in all cases.

| Set | | | I | II | III |
|---|---|---|---|---|---|
| Central | $V$ | (MeV) | 290 | 290 | 290 |
| Real | $r$ | (fm) | 1.175 | 1.175 | 1.175 |
| | $a_r$ | (fm) | 0.64 | 0.64 | 0.64 |
| Deformation | $\beta_V$ | | | | −0.1 |
| Central | $W$ | (MeV) | 10.71 | 10.71 | 10.71 |
| Imaginary | $r_W$ | (fm) | 2.24 | 2.24 | 2.24 |
| | $a_W$ | (fm) | 0.97 | 0.97 | 0.97 |
| Deformation | $\beta_W$ | | | | −0.1 |
| Real | $V_{LS}$ | (MeV) | 1.75 | 1.9 | 0.15 |
| spin-orbit | $r_{LS}$ | (fm) | 1.2 | 1.15 | 2.2 |
| | $a_{LS}$ | (fm) | 0.45 | 0.05 | 0.04 |
| Imaginary | $W_{LS}$ | (MeV) | | | 0.2 |
| spin-orbit | $r_{W_{LS}}$ | (fm) | | | 2.2 |
| | $a_{W_{LS}}$ | (fm) | | | 0.04 |
| Third rank | $V_{T_3}$ | (MeV) | | 0.8 | 0.8 |
| tensor | $r_{T_3}$ | (fm) | | 0.6 | 0.6 |
| | $a_{T_3}$ | (fm) | | 0.05 | 0.04 |

A similar situation occurred with the third-rank tensor analyzing powers. The central plus third-rank tensor potential alone was able to provide a good description of the third rank tensor potentials $^TT_{30}$, $iT_{32}$, and $iT_{33}$ but was not able to describe $iT_{31}$. The introduction of a second-rank tensor potential destroyed this agreement. However, the inclusion of a real spin-orbit potential enabled a reasonable description of both the vector and third-rank tensor analyzing powers. The parameters of this potential are given as set II of Table I, while the resultant cross section and analyzing powers are denoted by the dotted curve in Fig. 2.

As no combination of spin-orbit and second- and third-rank tensor potentials seemed able to satisfactorily describe all the analyzing powers simultaneously, the effect of including a quadrupole deformed potential was investigated. Such a deformed potential does not imply any couplings due to reorientation of the ground state or to the first excited state of $^7$Li. It arises merely from the quadrupole deformed shape of $^7$Li, as described in Ref. [12]. Deformed real and imaginary central and spin-orbit potentials were investigated, and the best overall compromise fit was obtained with deformed real and imaginary central potentials of deformation $\beta=-0.1$ in addition to the standard central, real and imaginary spin-orbit and real third-rank tensor potentials. The parameters of this potential are given as set III of Table I, and the results are compared with the data in Fig. 2, where they are denoted by the solid curve.

A key as to the reason for the failure of the optical model calculations can be seen in Fig. 1, where previously mea-

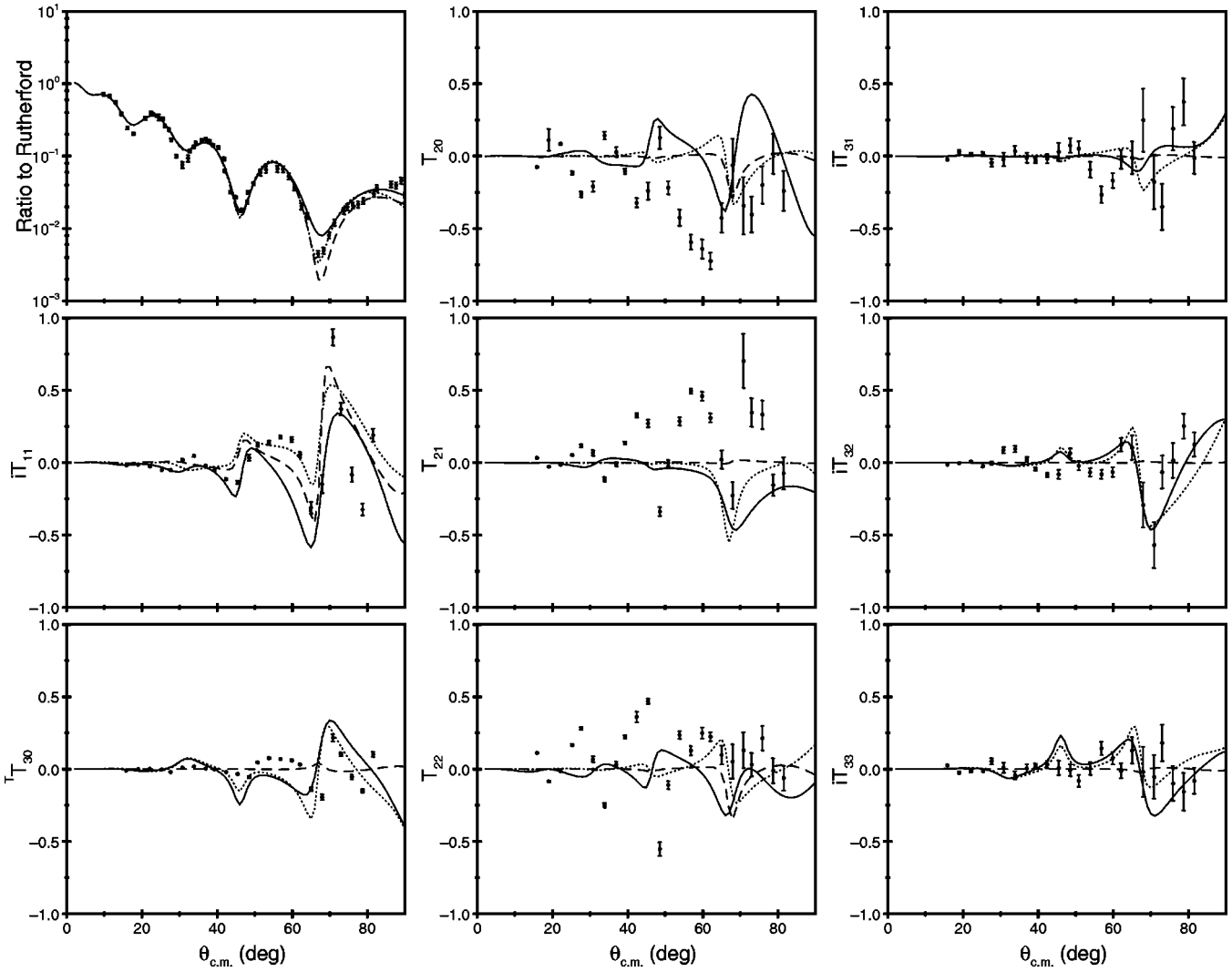


FIG. 2. Optical model fits compared to the data. The dashed curve denotes the best fit obtained to $iT_{11}$ with a real spin-orbit potential, while the dotted curve denotes the best simultaneous fit obtained to the vector and third-rank analyzing powers using real spin-orbit and third-rank tensor potentials. The solid curve denotes the best overall optical model fit to the data, where the optical model potential contains standard and quadrupole deformed real and imaginary central components and real and imaginary spin-orbit and real third rank tensor potentials.

sured cross section and analyzing power data for 30 MeV $^{6}$Li+$^{12}$C [6] and the present 34 MeV $^{7}$Li+$^{12}$C are compared. The primary difference between the two data sets is in the very large second rank tensor analyzing powers for $^{7}$Li scattering. It has been possible to describe the much smaller $^{6}$Li second-rank analyzing powers with a standard Raynal potential, so that it might be expected that this potential would not be able to describe the much larger $^{7}$Li analyzing powers.

## IV. CDCC CALCULATIONS

The CDCC calculations were performed using the code FRESCO [17], version FRXP.14. The method used was similar to that employed previously for a study of near-barrier $^{6,7}$Li breakup in the field of a $^{208}$Pb target [18]. Couplings between the $\alpha$-$t$ cluster states in $^{7}$Li were generated using the CF model, and included both nuclear and Coulomb form factors. Coupling to the $1/2^{-}$ bound state at 0.478 MeV, the $7/2^{-}$ and $5/2^{-}$ $L=3$ resonances at 4.63 and 6.68 MeV respectively and the $L=0,1,3$ nonresonant $\alpha$-$t$ continuum were included. Coupling to the $L=2$ continuum was omitted as it has previously been found to have little effect on the elastic scattering [18].

The nonresonant $\alpha$-$t$ continuum above the breakup threshold was discretized into a series of momentum bins with respect to the momentum $\hbar k$ of the $\alpha$-$t$ relative motion, the wave functions for these bins being normalized to unity. The radius limiting the range of the wave functions was set at 30 fm and the number of partial waves included in the calculations was limited to $l=60\hbar$. The continuum model space was as used previously [18], $k$ being limited to $0.0 \leqslant k \leqslant 0.75$ fm$^{-1}$ with $\Delta k=0.25$ fm$^{-1}$. The lowest, $0.0 \leqslant k \leqslant 0.25$ fm$^{-1}$, bins were omitted from all but the $L=0$ continuum, as these bins are found to have little effect on the elastic scattering and do not contribute significantly to the

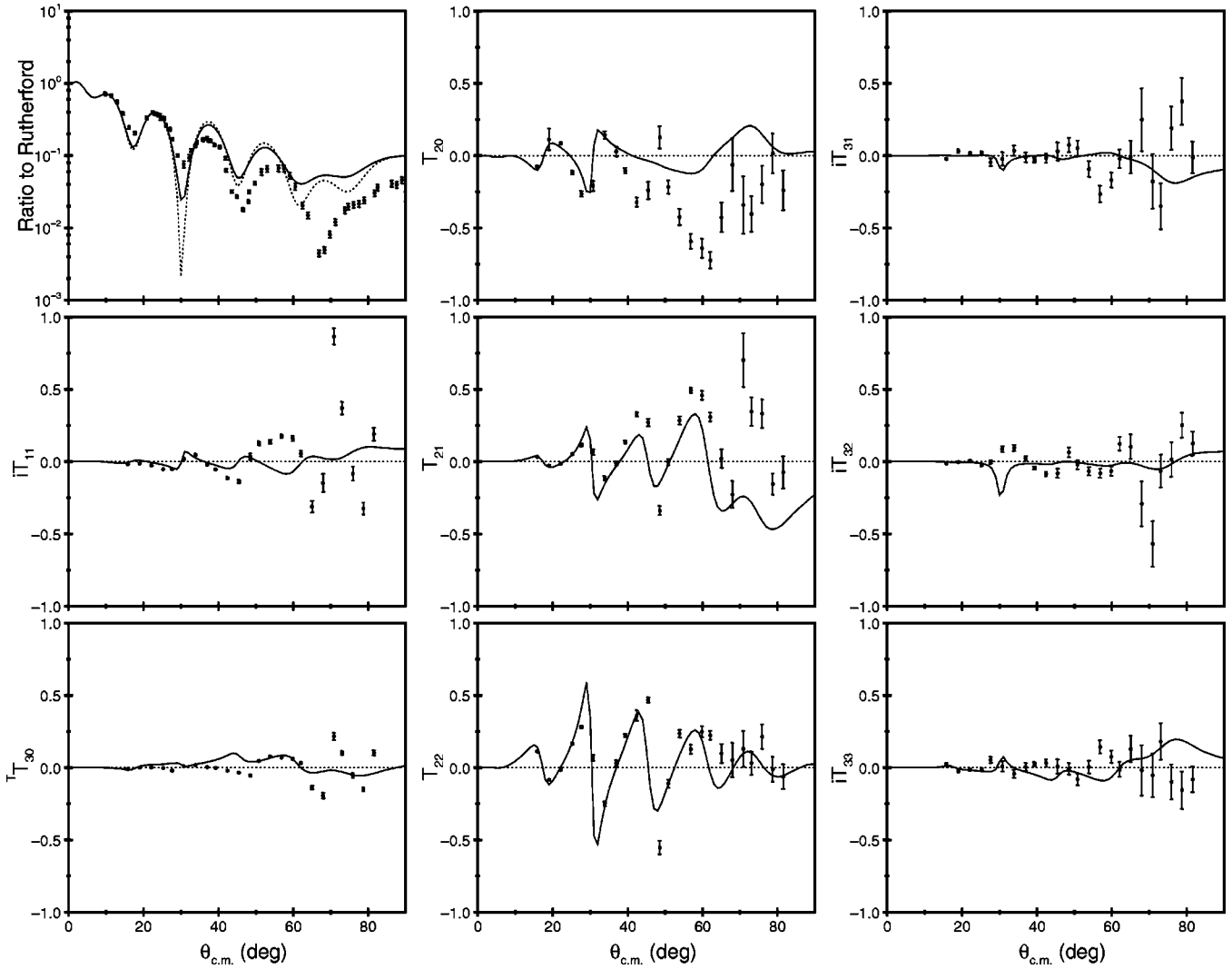


FIG. 3. Single channel CF model calculations. The solid curve shows the result of a calculation including ground-state reorientation, while the dotted curve shows the result with no reorientation.

total breakup cross section. The $L=3$ resonances were also treated as momentum bins, of sufficient width to accommodate the main strength of the resonances. These widths were 0.2 and 2.0 MeV for the $7/2^-$ and $5/2^-$ resonances respectively.

The same $\alpha$-$t$ binding potential, that of Buck and Merchant [19], was used to generate all the form factors. For the ground-state and first excited state the potential depth was adjusted to give the correct binding energy, while for the resonances it was adjusted to give a resonance at the correct energy. The $\alpha$-$^{12}$C potential was that of Ober and Johnson [20] and the $t$-$^{12}$C potential was that of Schmelzbach *et al.* [21]. As the CF model requires $\alpha$-target and $t$-target optical potentials at 4/7 and 3/7 of the $^7$Li bombarding energy respectively (19.43 and 14.57 MeV here) and the potentials used are for bombarding energies of 18 and 15 MeV, the real and imaginary potential strengths were treated as parameters that were adjusted to give the best fit to the elastic scattering cross section. This was achieved with renormalization factors of 0.4 and 0.9 for the real and imaginary potential strengths, respectively.

In order to investigate the effect of the ground state reorientation coupling alone, we initially carried out a single channel calculation that included just this coupling. The result is shown in Fig. 3 as the solid curve. For comparison, we also give the result of a single channel calculation without reorientation (the dotted curve in Fig. 3). As this calculation contains just a central optical potential with no couplings, no analyzing powers are generated. We also performed a four channel calculation, including couplings to the first excited state and $7/2^-$ and $5/2^-$ resonances of $^7$Li only. The results are shown in Fig. 4 as the dashed curve, where they may be compared with the results of the full calculation, denoted by the solid curve, allowing the effect of coupling to the $\alpha$-$t$ continuum to be seen. The dotted curve in Fig. 4 shows the effect of switching off the reorientation couplings in the full calculation.

Since the $^{12}$C target has a low-lying, strongly coupled $2^+$ excited state at an excitation energy of 4.44 MeV, it might be expected that coupling to this state would have an effect on the elastic scattering cross section and analyzing powers. However, calculations that included coupling to the $2^+$ state

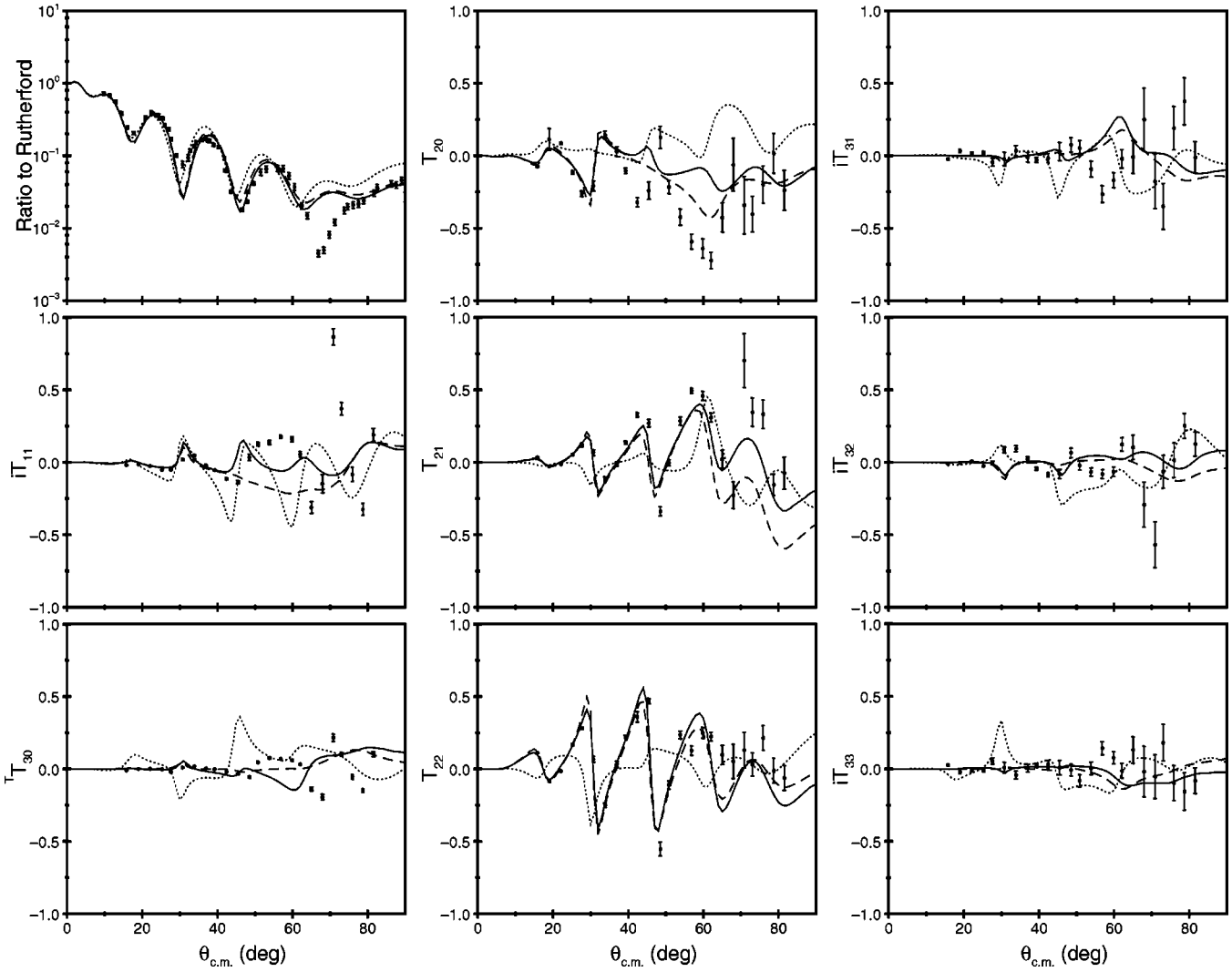


FIG. 4. Comparison of the CDCC calculations with the data. The solid curve denotes the full calculation, including couplings to the $1/2^-$ state, the $7/2^-$ and $5/2^-$ resonances, and the $L=0,1,3$ continuum and all reorientation couplings. The dotted curve denotes the same calculation, but with reorientation couplings omitted. The dashed curve denotes the four channel calculation, including couplings to the $1/2^-$ state and $7/2^-$ and $5/2^-$ resonances only.

in addition to the full CDCC model space for $^7$Li found that both the cross section and analyzing powers were essentially unchanged in the angular range $0°-90°$ (for angles greater than about 100° the cross section is considerably altered by the $2^+$ coupling, but the analyzing powers remain essentially unchanged except at extreme backward angles).

## V. DISCUSSION

It is clear from Fig. 2 that while optical model calculations are able to produce a reasonably good simultaneous fit to the elastic scattering cross section and vector and third-rank tensor analyzing powers, they are unable to satisfactorily describe the second-rank tensor analyzing powers. Any attempt to generate second-rank tensor analyzing powers of sufficient amplitude to match the data by the introduction of a second-rank tensor potential merely resulted in destroying the previous agreement with the vector and third-rank tensor analyzing powers. A similar effect was observed by Moroz *et al.* [8] in their analysis of first- and second-rank analyzing powers for $^{12}$C($^7\vec{\text{Li}}$,$^7$Li)$^{12}$C at a bombarding energy of 21.1 MeV. They also found that any second-rank tensor potential that was able to generate second-rank tensor analyzing powers of similar amplitude to those observed destroyed the vector analyzing powers generated by a spin-orbit potential. They were also unable to find a combination of standard spin-orbit and second-rank tensor potentials that provided a simultaneous good fit to the first- and second-rank analyzing powers.

The introduction of quadrupole deformed real and imaginary central potentials generated some structure in the second-rank analyzing powers without destroying the previous agreement with the measured vector and third-rank tensor analyzing powers, but the agreement with the data is still far from satisfactory. The results of the optical model analy sis suggest that whatever the mechanism that generates the second-rank tensor analyzing powers, it cannot be represented by a second-rank tensor potential of standard Raynal

form if we are to simultaneously describe the cross section and other analyzing powers.

As Table I shows, the diffuseness parameters of the spin-orbit and third-rank tensor potentials of sets II and III are such that these potentials are essentially of square-well form. The small diffuseness of the third rank tensor potential was found to be necessary to generate the sharp dip seen at about 70° in $iT_{32}$ and $iT_{33}$. The validity of these small diffuseness parameters was checked by performing the optical model calculations with integration step sizes from 0.1 fm to 0.05 fm. In each case the cross section and analyzing powers produced varied little from those found with a step size of 0.1 fm.

The optical model calculations show some evidence for a third-rank potential of the form suggested by Mukhopadhyay *et al.* [15], as the spin-orbit potential that provides the best description of $iT_{11}$ does not generate third-rank analyzing powers. However, this is a weak conclusion, due to our inability to describe the second-rank tensor analyzing powers. It is possible that, if we were able to find a second-rank tensor potential that was able to fit the second-rank analyzing powers without destroying the agreement with $iT_{11}$, an explicit third-rank potential would not be required to fit the third-rank analyzing powers.

As Fig. 4 shows, the full CDCC calculation provides a reasonable overall description of the elastic scattering cross section and analyzing powers, the second-rank tensor analyzing powers being particularly well described. However, a notable failure of the calculation is the inability to generate the large peak in $iT_{11}$ at about 70°, suggesting that a process or processes other than excitation of $^{7}$Li are important in the generation of this analyzing power. This is probably linked to the inability of the calculation to describe the interference dip seen in the elastic scattering cross section at the same angle.

Similar results were found by Sakuragi *et al.* [22] who performed CDCC calculations using double folding model form factors for $^{7}$Li+$^{12}$C at 21.1 MeV. They were able to obtain a good description of the second-rank analyzing powers (although, as is the case here, $T_{20}$ was somewhat less well described than $T_{21}$ and $T_{22}$) with a poorer description of the vector analyzing power $iT_{11}$. Although their description of $iT_{11}$ is rather better than ours, the agreement begins to deteriorate at larger angles. This is similar to our calculation, that describes $iT_{11}$ well at angles $<40°$. However, the calculations of Sakuragi *et al.* provide a good description of $iT_{11}$ out to much larger angles. This suggests that the mechanism(s) that generate $iT_{11}$ are poorly understood in the region where nuclear effects dominate, as this should begin at smaller angles as the bombarding energy is increased.

In general the third-rank analyzing powers are rather poorly described, except at the smallest angles where they are essentially zero. The overall description is reasonable, except for $iT_{31}$ at about 50° where the sign is wrong, but the details of the angular structure are not described. Thus, as for $iT_{11}$, we cannot claim to understand the mechanism(s) that generate the third-rank analyzing powers. Based on the current calculations, there are processes other than couplings to the excited states and $\alpha$-$t$ continuum of $^{7}$Li that are important contributors to the generation of these analyzing powers. Calculations that included coupling to the 4.44 MeV $2^{+}$ state of $^{12}$C produced results that were essentially unchanged, indicating that this coupling has little influence on the generation of the analyzing powers.

The omission of the reorientation couplings has a profound effect on the analyzing powers produced by the CDCC calculation, as may be seen by a comparison of the solid and dotted curves in Fig. 4. The effect on the cross section of omitting the reorientation couplings can be largely compensated for by further renormalization of the CF model real potential strength. However, the same is not true for the analyzing powers, indicating that the inclusion of reorientation couplings is essential for an accurate description of the polarization observables and suggesting that this coupling cannot be adequately represented by a simple DPP.

Due to the large quadrupole moment of $^{7}$Li it was anticipated that ground state reorientation would play a major part in the effect of the reorientation couplings as a whole. In Fig. 3 it can be seen that this is indeed the case. Coupling to the ground state reorientation alone produces significant first-, second-, and third-rank analyzing powers. However, the main effect is in the second-rank tensor analyzing powers, which on comparison of Fig. 3 with Fig. 4 shows are almost entirely produced by the ground-state reorientation coupling. Thus, our calculations indicate that the ground-state reorientation coupling remains in the main source of the second rank tensor analyzing powers in $^{7}$Li elastic scattering at higher relative bombarding energies. This result has important implications for nuclei such as $^{8}$B and $^{9}$Be that also have large ground state quadrupole moments [$Q(^{7}\mathrm{Li}) = -40.0 \pm 0.6$ mb [23], $Q(^{8}\mathrm{B}) = 68.3 \pm 2.1$ mb [24], $Q(^{9}\mathrm{Be}) = 53 \pm 3$ mb [25]]. With the current tendency towards more microscopic descriptions of data, as in recent work on $^{8}$B [26–31], for example, it is important to take the reorientation couplings into account if one is to fully understand the reactions of such nuclei. The current work suggests that this is particularly important in the analysis of elastic scattering and fusion data using microscopic models.

The other couplings have most effect on the third-rank tensor analyzing powers and the vector analyzing power $iT_{11}$. The effect of coupling to the $\alpha$-$t$ continuum is demonstrated in Fig. 4 by a comparison of the solid and dashed curves. Here it can be seen that while the effect on the elastic scattering cross section of coupling to the continuum is negligible in the angular range 0°–90°, the effect of this coupling on the analyzing powers can be quite large. It is most notable in $iT_{11}$, $^{T}T_{30}$, $T_{20}$, and at angles beyond about 60° in $T_{21}$. This provides a clear demonstration of the importance of including continuum couplings for an accurate description of polarization observables. Sakuragi *et al.* [22] also found a significant effect on the analyzing powers due to coupling to the $\alpha$-$t$ continuum in CDCC calculations for 44 MeV $^{7}$Li+$^{26}$Mg and 21.1 MeV $^{7}$Li+$^{12}$C elastic scattering.

To summarize, a complete set of elastic scattering analyzing powers for the $^{7}$Li+$^{12}$C system at a bombarding energy of 34 MeV was presented. Extensive optical model searches using spin orbit and second and third-rank tensor potentials of standard forms have failed to find a potential that gives a

simultaneous good fit to all the analyzing powers and the cross section, the main problem being an inability to describe the second-rank analyzing powers without destroying the agreement with the first and third ranks. In contrast, CDCC calculations using CF model form factors are able to provide a reasonable overall description of the data (with the exception of $iT_{11}$ and $iT_{31}$ beyond about 40°). Further CDCC calculations suggest that coupling to the ground-state reorientation is the main source of the polarization observables, particularly the second-rank tensor analyzing powers. This, together with the failure of conventional optical model forms to fit the data, in turn suggests that the complete effect of this reorientation coupling on the elastic scattering cannot be simulated by a dynamic polarization potential of the usual form. Our calculations also clearly demonstrate the importance of the effect of coupling to the $\alpha$-$t$ continuum on the analyzing powers for this system. By contrast, coupling to the $^{12}$C $2^+$ state at 4.44 MeV had little effect on the results.

## ACKNOWLEDGMENTS

The authors wish to acknowledge many enlightening discussions with Professor D. Robson. This work was supported by the State of Florida, the U.S. National Science Foundation, the State Committee for Scientific Research (KBN) of Poland, and a CLG NATO grant.

[1] E.E. Bartosz, P.D. Cathers, K.W. Kemper, F. Maréchal, D. Robson, G. Grawert, and K. Rusek, Phys. Lett. B **488**, 138 (2000).
[2] G. Tungate, D. Krämer, R. Butsch, O. Karban, K.-H. Möbius, W. Ott, P. Paul, A. Weller, E. Steffens, K. Becker, K. Blatt, D. Fick, B. Heck, H. Jänsch, H. Leucker, K. Rusek, I.M. Turkiewicz, and Z. Moroz, J. Phys. G **12**, 1001 (1986).
[3] W. Ott, R. Butsch, H.J. Jänsch, K.-H. Möbius, P. Paul, G. Tungate, E. Steffens, K. Rusek, Z. Moroz, I.M. Turkiewicz, K. Becker, K. Blatt, H. Leucker, and D. Fick, Nucl. Phys. **A489**, 329 (1988).
[4] P.D. Cathers, E.E. Bartosz, M.W. Cooper, N. Curtis, N. Keeley, K.W. Kemper, F. Maréchal, E.G. Myers, B.G. Schmidt, K. Rusek, and V. Hnizdo, Phys. Rev. C **63**, 064601 (2001).
[5] V. Hnizdo, K.W. Kemper, and J. Szymakowski, Phys. Rev. Lett. **46**, 590 (1981).
[6] E.L. Reber, K.W. Kemper, P.V. Green, P.L. Kerr, A.J. Mendez, E.G. Meyers, B.G. Schmidt, and V. Hnizdo, Phys. Rev. C **50**, 2917 (1994).
[7] K. Rusek, Z. Moroz, R. Čaplar, P. Egelhof, K.-H. Möbius, E. Steffens, I. Koenig, A. Weller, and D. Fick, Nucl. Phys. **A407**, 208 (1983).
[8] Z. Moroz, K. Rusek, P. Egelhof, S. Kossionides, K.-H. Mobius, G. Tungate, E. Steffens, G. Grawert, I. Koenig, and D. Fick, Nucl. Phys. **A417**, 498 (1984).
[9] K. Rusek, J. Giroux, H. Jänsch, H. Vogt, K. Becker, K. Blatt, A. Gerlach, W. Korsch, H. Leucker, W. Luck, H. Reich, H.-G. Völk, and D. Fick, Nucl. Phys. **A503**, 223 (1989).
[10] P.D. Cathers, P.V. Green, E.E. Bartosz, K.W. Kemper, F. Maréchal, E.G. Myers, and B.G. Schmidt, Nucl. Instrum. Methods Phys. Res. A **457**, 509 (2001).
[11] A.J. Mendez, E.G. Myers, K.W. Kemper, P.L. Kerr, E.L. Reber, and B.G. Schmidt, Nucl. Instrum. Methods Phys. Res. A **329**, 37 (1993).
[12] J. Cook, Comput. Phys. Commun. **31**, 363 (1984).
[13] J. Raynal, Phys. Lett. **7**, 281 (1963).
[14] M. Irshad and B.A. Robson, Nucl. Phys. **A218**, 504 (1974).
[15] D. Mukhopadhyay, G. Grawert, D. Fick, and Z. Moroz, Phys. Lett. **104B**, 361 (1981).
[16] M.F. Vineyard, J. Cook, K.W. Kemper, and M.N. Stephens, Phys. Rev. C **30**, 916 (1984).
[17] I.J. Thompson, Comput. Phys. Rep. **7**, 167 (1988).
[18] N. Keeley and K. Rusek, Phys. Lett. B **427**, 1 (1998).
[19] B. Buck and A.C. Merchant, J. Phys. G **14**, L211 (1988).
[20] D.R. Ober and O.E. Johnson, Phys. Rev. **170**, 924 (1968).
[21] P.A. Schmelzbach, R.A. Hardekopf, R.F. Haglund, Jr., and G.G. Ohlsen, Phys. Rev. C **17**, 16 (1978).
[22] Y. Sakuragi, M. Yahiro, M. Kamimura, and M. Tanifuji, Nucl. Phys. **A480**, 361 (1988).
[23] M. Urban and A.J. Sandlej, Chem. Phys. Lett. **173**, 157 (1990); H.-G. Voelk and D. Fick, Nucl. Phys. **A530**, 475 (1991).
[24] T. Minamisono, T. Ohtsubo, I. Minami, S. Fukuda, A. Kitagawa, M. Fukuda, K. Matsuta, Y. Nojiri, S. Takeda, H. Sagawa, and H. Kitagawa, Phys. Rev. Lett. **69**, 2058 (1992).
[25] F. Ajzenberg-Selove, Nucl. Phys. **A490**, 1 (1988).
[26] H. Esbensen and G.F. Bertsch, Nucl. Phys. **A600**, 37 (1996).
[27] R. Shyam and I.J. Thompson, Phys. Rev. C **59**, 2645 (1999).
[28] F.M. Nunes and I.J. Thompson, Phys. Rev. C **59**, 2652 (1999).
[29] H. Esbensen and G.F. Bertsch, Phys. Rev. C **59**, 3240 (1999).
[30] V. Guimarães, J.J. Kolata, D. Peterson, P. Santi, R.H. White-Stevens, S.M. Vincent, F.D. Becchetti, M.Y. Lee, T.W. O'Donnell, D.A. Roberts, and J.A. Zimmerman, Phys. Rev. Lett. **84**, 1862 (2000).
[31] J.A. Tostevin, F.M. Nunes, and I.J. Thompson, Phys. Rev. C **63**, 024617 (2001).